N70-42092

NASA TECHNICAL MEMORANDUM

NASA TM X-2071

NASA TM X-2071

FREE-FLIGHT MEASUREMENTS OF DYNAMIC STABILITY DERIVATIVES OF A BLUNTED 120° CONE IN HELIUM AT MACH NUMBER 15.4

by Frederick W. Gibson and James E. Carter

Langley Research Center
Hampton, Va. 23365

NATIONAL AERONAUTICS AND SPACE ADMINISTRATION • WASHINGTON, D. C. • OCTOBER 1970

1. Report No.	2. Government Accession No.	3. Recipient's Catalog No.
NASA TM X-2071		

4. Title and Subtitle	5. Report Date
FREE-FLIGHT MEASUREMENTS OF DYNAMIC STABILITY DERIVATIVES OF A BLUNTED 120° CONE IN HELIUM AT MACH NUMBER 15.4	October 1970
	6. Performing Organization Code
7. Author(s) Frederick W. Gibson and James E. Carter	8. Performing Organization Report No. L-6883
	10. Work Unit No. 124-08-13-01
9. Performing Organization Name and Address NASA Langley Research Center Hampton, Va. 23365	11. Contract or Grant No.
	13. Type of Report and Period Covered Technical Memorandum
12. Sponsoring Agency Name and Address National Aeronautics and Space Administration Washington, D.C. 20546	14. Sponsoring Agency Code

15. Supplementary Notes

16. Abstract

The dynamic stability derivatives of a blunted 120° cone with different center-of-gravity locations for various amplitudes of oscillation were determined at a Mach number of 15.4 in helium. A free-flight method was utilized and the data thus acquired are compared with unmodified Newtonian theory predictions and experimental results obtained in air.

17. Key Words (Suggested by Author(s))	18. Distribution Statement
Free-flight measurements Dynamic stability Air-helium simulation Hypersonic flow	Unclassified – Unlimited

19. Security Classif. (of this report)	20. Security Classif. (of this page)	21. No. of Pages	22. Price*
Unclassified	Unclassified	22	$3.00

*For sale by the Clearinghouse for Federal Scientific and Technical Information
Springfield, Virginia 22151

FREE-FLIGHT MEASUREMENTS OF DYNAMIC STABILITY DERIVATIVES OF A BLUNTED 120° CONE IN HELIUM AT MACH NUMBER 15.4

By Frederick W. Gibson and James E. Carter
Langley Research Center

SUMMARY

An investigation has been made to determine the dynamic stability derivatives of a blunted 120° cone for various amplitudes of oscillation and center-of-gravity locations at a Mach number of 15.4 in helium. The data were obtained by utilizing a free-flight method and these data are compared with those predicted by unmodified Newtonian theory and experimental results obtained in air.

INTRODUCTION

Considerable effort has been expended (e.g., see refs. 1 to 3) to understand under what conditions helium data can be expected to be indicative of results that would be obtained in air. Nevertheless, it is not known whether hypersonic helium data can be used in the prediction of supersonic characteristics of large-angle blunted cones in air. The aim of this investigation was to examine the air-helium simulation problem for a 120° blunted-nose cone as well as to provide additional dynamic stability data for this configuration. A wind-tunnel free-flight technique was employed in a Mach 15.4 helium flow to obtain stability coefficients free of sting effects. This technique is reported in detail in references 4 to 7. The models were constructed of a fiber-glass shell filled with plastic foam and had a lead slug extending from the nose to various locations along the axis of symmetry. The models were launched at various angles of attack and propelled upstream by a pneumatic launcher. High-speed motion pictures were taken of the flight upstream and return, and from these the basic time-dependent attitude data were obtained.

SYMBOLS

C_D drag coefficient, $\dfrac{\text{Drag force}}{q_\infty S}$

C_L lift coefficient, $\dfrac{\text{Lift force}}{q_\infty S}$

C_{L_α}	lift-coefficient slope per radian
C_m	pitching-moment coefficient, $\frac{\text{Pitching moment}}{q_\infty S d}$
C_{m_α}	pitching-moment coefficient slope per radian
$C_{m_q} + C_{m_{\dot\alpha}}$	dynamic-stability coefficient, assumed constant over an oscillation cycle, $\frac{\partial C_m}{\partial \frac{\dot\theta d}{V}} + \frac{\partial C_m}{\partial \frac{\dot\alpha d}{V}}$
C_p	pressure coefficient, $\frac{p - p_\infty}{q_\infty}$
d	model base diameter
I	model moment of inertia about a transverse axis at center of gravity
M_∞	free-stream Mach number
m	mass of model
n	number of cycles
p	static pressure
p_∞	free-stream static pressure
$p_{t,\infty}$	free-stream total pressure
q_∞	free-stream dynamic pressure
r	radius
r_b	radius of base
r_n	radius of nose

S	model base area, $\pi d^2/4$
t	time
V	model velocity relative to medium
V_i	model velocity relative to inertial system
V_∞	free-stream velocity
X,Z	axis system fixed with respect to moving medium
x	model position relative to medium along tunnel center line
x_{cg}	distance from model nose to center of gravity divided by the total body length
z	model position in vertical direction relative to tunnel center line
α	model angle of attack as defined in figure 7
γ	ratio of specific heats
θ	pitch angle as defined in figure 7
$\overline{\theta}$	root mean square of θ as defined by equation (8)
θ_o	value of θ at $t = 0$
θ_n	value of θ at the end of n cycles
ρ_∞	free-stream density
ω	circular frequency

An arrow over a symbol denotes a vector.

A dot over a symbol denotes a derivative with respect to time.

APPARATUS AND TESTS

The tests were conducted in the 24-inch-diameter (60.96-cm) nozzle of the Mach 15 helium flow apparatus at the Langley Research Center. This blowdown-type tunnel, which operates at an average test-section Mach number of 15.4, is described in reference 8. For the present study, the stagnation pressures ranged from approximately 234 to 330 psia (1.61 to 2.28 MN/m^2), stagnation temperatures from 70° to 80° F (294° to 300° K), and Reynolds numbers from 1.65×10^6 to 2.33×10^6 per foot (5.41×10^6 to 7.64×10^6 per meter).

The launcher which was used to propel the models upstream is shown in the photograph of figure 1 and schematically in figure 2. The model was launched at a predetermined initial angle, velocity, and tunnel stagnation pressure.

MODELS

The models were blunted 120° cones with a base diameter of 3 inches (7.62 cm) and with nose and shoulder radii 0.125 and 0.04 times the base diameter, respectively. The model construction was as shown in figure 3, that is, foam-filled fiber-glass shells with a lead slug symmetrical with the axis of symmetry for ballast and to change the center-of-gravity location. The launch angle of attack was built into the model as indicated in figure 3. An analytical balance was used to determine the mass of the models, and the moment of inertia was determined by use of a torsion pendulum. The moment of inertia was calculated for calibration bodies and the periods of these bodies were determined experimentally by use of the device shown in figure 4. The periods of the models were then obtained in a similar manner, and the moments of inertia were obtained from the calibration curve of I as a function of the square of the period for the calibration bodies. The positions of the centers of gravity were obtained by use of the device shown in figures 1 and 4. The physical properties of the models and test parameters used in the experiment are given in table I.

DATA REDUCTION

The raw data were obtained from motion pictures taken of the flight in both the vertical and horizontal planes, and consisted of time histories of translational position and oscillation amplitude of the model. A series of motion-picture frames from a typical test is shown in figure 5, and a plot of the data from another flight is shown in figure 6. For the tests reported herein the model motion was planar, although the plane of motion was inclined with respect to the horizontal and vertical planes, as shown in the typical photographs of figure 5. Only the tests for which at least two cycles of planar motion were observed are reported herein. The data acquired should be considered qualitative only, as it was not possible to determine the degree of uncertainty in the measurements because of the small damping which the models demonstrated and the difficulties encountered in repeating tunnel operating conditions.

The data-reduction technique used in this analysis is described in reference 7 and a brief description is given in the following sections. For convenience, a detailed derivation of the equations used to obtain the experimental drag and stability coefficients is given in the appendix.

Drag

The coordinate system used for the data reduction references the model position to the moving gas; figure 7 (from ref. 7) shows this coordinate system. The distance between the model and the moving medium is x and it is the independent variable for the equations of motion. The drag coefficient can be obtained from the translational equation of motion:

$$m \frac{d^2x}{dt^2} = -\frac{1}{2} \rho_\infty V^2 S C_D \tag{1}$$

After rearranging equation (1) and changing the independent variable from time to distance, the following equation for the drag coefficient results:

$$C_D = -\frac{2m}{\rho_\infty S} \frac{d\left[\ln\left(1 + \frac{V_i}{V_\infty}\right)\right]}{dx} \tag{2}$$

A linear fit through the data for $\ln\left(1 + \frac{V_i}{V_\infty}\right)$ as a function of x yields an effective drag coefficient valid over several cycles of the oscillatory motion. A representative plot of $\ln\left(1 + \frac{V_i}{V_\infty}\right)$ against x is shown in figure 8.

Static Stability

The solution to the linearized equation of planar angular motion (i.e., linear aerodynamic coefficients $C_m = C_{m_\alpha}\alpha$, $C_L = C_{L_\alpha}\alpha$, and $C_D = \text{Constant}$) is

$$\theta = \theta_0 e^{\lambda x} \cos\left[\left(-\frac{\rho_\infty S d}{2I} C_{m_\alpha} + \lambda^2\right)^{1/2} x\right] \tag{3}$$

where θ is a function of the distance x and

$$\lambda = \frac{\rho_\infty S}{4m}\left[C_D - C_{L_\alpha} + \frac{md^2}{I}\left(C_{m_q} + C_{m_{\dot\alpha}}\right)\right]$$

In general, $-\frac{\rho_\infty Sd}{2I} C_{m_\alpha} >> \lambda^2$, and hence equation (3) becomes

$$\theta = \theta_o e^{\lambda x} \cos\left[\left(-\frac{\rho_\infty Sd}{2I} C_{m_\alpha}\right)^{1/2} x\right] \tag{4}$$

If, in equation (4), x is replaced by $V_\infty t$, then C_{m_α} can readily be related to the circular frequency of motion ω as follows:

$$C_{m_\alpha} = -\frac{I\omega^2}{q_\infty Sd} \tag{5}$$

which yields an effective constant pitching-moment slope valid over several cycles of the oscillatory motion.

Dynamic Stability

The experimental dynamic-stability coefficient $C_{m_q} + C_{m_{\dot\alpha}}$ was obtained from the amplitude envelope

$$\theta = \theta_o e^{\lambda x} \tag{6}$$

Inserting the definition of λ in equation (6) and evaluating at the end of n cycles $\left(\text{i.e., replacing } x \text{ with } x \approx \frac{2\pi n V_\infty}{\omega} \text{ and setting } \theta = \theta_n\right)$ leads to the following equation:

$$C_{m_q} + C_{m_{\dot\alpha}} = \frac{I\omega V_\infty}{q_\infty Sd^2} \frac{1}{\pi n} \ln \frac{\theta_n}{\theta_o} + \frac{I}{md^2}\left(C_{L_\alpha} - C_D\right) \tag{7}$$

It should be noted that values of C_{L_α} were not obtained in the present experimental investigation. However, an experimentally determined value of C_{L_α} was taken from reference 9. This value was obtained in air and is discussed subsequently.

Data-Correlation Parameter

The root mean square or the amplitude envelope was used to correlate the data. If the root mean square is defined as $\bar\theta$,

$$\bar{\theta}^2 = \frac{\int_0^x \theta^2 \, dx}{x} \tag{8}$$

Substitution of equation (6) into equation (8) and integrating through n cycles yields

$$\bar{\theta} = \left[\frac{\theta_n{}^2 - \theta_o{}^2}{\ln\left(\frac{\theta_n}{\theta_o}\right)^2}\right]^{1/2} \tag{9}$$

THEORETICAL CONSIDERATIONS

Air-Helium Simulation

The air-helium simulation problem has been considered (e.g., see refs. 1 to 3), but at the present time the findings are still incomplete, particularly for large-angle blunted cones. Figure 9 presents the calculated pressure distribution at zero angle of attack on the surface of the models for helium flow at $M_\infty = 15.4$ and for the air flow at $M_\infty = 3.0$, 4.0, and 5.0. These theoretical calculations were made with the computer program given in reference 10. The agreement between the air results at $M_\infty = 3.0$ and the helium results at $M_\infty = 15.4$ is excellent. This result partially justifies the use in equation (7) of the experimental value of C_{L_α} obtained in air, and correspondingly allows the comparison of stability data for a 120° blunted cone under the same conditions.

Stability-Derivative Calculations

The theoretical dynamic and static stability derivatives were calculated by using equations developed from those in reference 11, which are based on unmodified Newtonian theory. It was found that the contribution of the spherical nose to these derivatives was very slight and, hence, could be ignored. The use of Newtonian theory is restricted to low values of oscillation frequency. In view of the relatively high frequencies of the present experiment, it was not expected that the dynamic stability derivative would be predicted accurately.

RESULTS AND DISCUSSION

The aerodynamic stability and drag data of the tests and the theoretical calculations are presented in tables I and II and figures 10 to 13. The drag data, as shown in figure 10, agrees well in magnitude both with that predicted by unmodified Newtonian theory and with the experimental result from reference 9 obtained at Mach 2.96 in air. In figures 11 and 12, the dynamic-stability coefficient $C_{m_q} + C_{m_{\dot{\alpha}}}$ is plotted as a function of mean amplitude and center-of-gravity position, respectively, and compared with the Newtonian results over the range of the experiments. The experimental values are considerably greater in magnitude than the Newtonian values; however, the present data is seen in figure 12 to have fair qualitative agreement with that from reference 12 (air data) extrapolated to the present center-of-gravity locations.

The static stability derivative is plotted as a function of center-of-gravity position in figure 13. The agreement with Newtonian theory is fair; however, the scatter in the experimental data precludes any conclusion that the static stability decreases as the center of gravity moves aft in the model – a trend which is predicted by Newtonian theory. Shown as a solid line in figure 13 are the C_{m_α} data obtained from reference 9 and transferred to the present range of center of gravity. The lack of better agreement with the present results is unexplained, although it is probably indicative of the breakdown of the air-helium simulation for a large-angle blunted cone at an angle of attack.

CONCLUDING REMARKS

The results of a study of the stability derivatives for a blunted 120° cone at $M_\infty = 15.4$ in helium have indicated that the free-flight technique employed is a useful tool for obtaining data free of sting effects. However, scatter in the data, particularly for the dynamic-stability coefficient, was too great to permit conclusions to be drawn regarding trends with center-of-gravity location and amplitude of oscillation. The measured values of the dynamic-stability coefficient were considerably greater in magnitude than the values predicted by unmodified Newtonian theory.

The lack of agreement of the present static-stability data obtained in helium with those previously obtained in air by other investigators (NASA TN D-4719) indicates that simulation of supersonic aerodynamic data with hypersonic helium data is not an efficacious technique for large-angle blunted cones.

Langley Research Center,
National Aeronautics and Space Administration,
Hampton Va., July 29, 1970.

APPENDIX

DERIVATION OF EQUATIONS

Drag Coefficient

The experimental drag coefficient is found from an equation which results from modifying the translational equation of motion:

$$-m\frac{d^2x}{dt^2} = \frac{1}{2}\rho_\infty V^2SC_D$$

$$-m\frac{dV}{dt} = \frac{1}{2}\rho_\infty V^2SC_D$$

$$-m\frac{d(\ln V)}{dt} = \frac{1}{2}\rho_\infty VSC_D \tag{A1}$$

and since

$$\frac{d}{dt} = \frac{dx}{dt}\frac{d}{dx} = V\frac{d}{dx}$$

then

$$-m\frac{d(\ln V)}{dx} = \frac{1}{2}\rho_\infty SC_D$$

or

$$C_D = -\frac{2m}{\rho_\infty S}\frac{d(\ln V)}{dx}$$

This equation can be rearranged as follows:

$$\frac{d(\ln V)}{dx} = \frac{d\left[\ln(V_\infty + V_i)\right]}{dx} = \frac{d\left\{\ln\left[V_\infty\left(1 + \frac{V_i}{V_\infty}\right)\right]\right\}}{dx} = \frac{d(\ln V_\infty)}{dx} + \frac{d\left[\ln\left(1 + \frac{V_i}{V_\infty}\right)\right]}{dx} = \frac{d\left[\ln\left(1 + \frac{V_i}{V_\infty}\right)\right]}{dx}$$

Hence, the final drag-coefficient equation for data reduction becomes

$$C_D = -\frac{2m}{\rho_\infty S}\frac{d\left[\ln\left(1 + \frac{V_i}{V_\infty}\right)\right]}{dx} \tag{A2}$$

Dynamic-Stability Coefficient

The equation of planar angular motion is

$$I\frac{d^2\theta}{dt^2} - \frac{1}{2}\rho_\infty V^2 Sd\left(C_{m_q} + C_{m_{\dot{\alpha}}}\right)\left(\frac{d}{V}\frac{d\theta}{dt}\right) - \frac{1}{2}\rho_\infty V^2 SdC_m = 0 \tag{A3}$$

Changing the independent variable from t to x and using the x translational equation (A1) gives

$$\frac{d}{dt} = \frac{dx}{dt}\frac{d}{dx} = V\frac{d}{dx}$$

$$\frac{d^2}{dt^2} = V\frac{d}{dx}\left(V\frac{d}{dx}\right) = V\frac{dV}{dx}\frac{d}{dx} + V^2\frac{d^2}{dx^2} = -\frac{\rho_\infty V^2 SC_D}{2m}\frac{d}{dx} + V^2\frac{d^2}{dx^2}$$

After assuming linear aerodynamics $\left(\text{that is, } C_L = C_{L_\alpha}\alpha, \quad C_D = \text{Constant, and } C_m = C_{m_\alpha}\alpha\right)$, the equation of motion becomes

$$\frac{d^2\theta}{dx^2} - \frac{\rho_\infty S}{2m}\left[C_D + \frac{md^2}{I}\left(C_{m_q} + C_{m_{\dot{\alpha}}}\right)\right]\frac{d\theta}{dx} - \frac{\rho_\infty Sd}{2I}C_{m_\alpha}\alpha = 0 \tag{A4}$$

It is now necessary to substitute $\alpha = f(\theta)$; this function is easily derived from the following equation which results from a small-angle assumption:

$$\alpha = \theta - \frac{1}{V}\frac{dz}{dt} \tag{A5}$$

If gravity is ignored, the vertical translational equation is

$$\frac{d^2z}{dt^2} = \frac{\rho_\infty V^2 SC_L}{2m} \tag{A6}$$

Since α and θ are nearly equal, it is permissible to set

$$C_L = C_L(\theta) \approx \frac{dC_L}{d\theta}\theta = \frac{dC_L}{d\alpha}\frac{d\alpha}{d\theta}\theta \approx C_{L_\alpha}\theta$$

which results in

$$\frac{dz}{dt} = \frac{\rho_\infty SC_{L_\alpha}}{2m}\int V^2\theta\, dt \tag{A7}$$

Since the motion is lightly damped, an approximate equation for angular motion is obtained from equation (A3) by setting $C_{m_q} + C_{m_{\dot{\alpha}}} = 0$. Again, since α and θ are nearly equal, $C_m \approx C_{m_\alpha}\theta$ and the resulting equation is:

$$I \frac{d^2\theta}{dt^2} = \frac{\rho_\infty V^2 Sd}{2} C_{m_\alpha}\theta \tag{A8}$$

Solving for θ from equation (A8) and substituting into equation (A7) yields

$$\frac{dz}{dt} = \frac{I}{md} \frac{C_{L_\alpha}}{C_{m_\alpha}} \frac{d\theta}{dt} \tag{A9}$$

and hence equation (A5) becomes

$$\alpha = \theta - \frac{I}{md} \frac{C_{L_\alpha}}{C_{m_\alpha}} \frac{1}{V} \frac{d\theta}{dt} \tag{A10}$$

If equation (A10) is substituted into equation (A4), the equation of motion becomes the following second-order differential equation with constant coefficients:

$$\frac{d^2\theta}{dx^2} - \frac{\rho_\infty S}{2m}\left[C_D - C_{L_\alpha} + \frac{md^2}{I}\left(C_{m_q} + C_{m_{\dot{\alpha}}}\right)\right]\frac{d\theta}{dx} - \frac{\rho_\infty Sd}{2I} C_{m_\alpha}\theta = 0 \tag{A11}$$

The solution to this equation is

$$\theta = \theta_0 e^{\lambda x} \cos\left[\left(-\frac{\rho_\infty Sd}{2I} C_{m_\alpha} + \lambda^2\right)^{1/2} x\right] \tag{A12}$$

where

$$\lambda = \frac{\rho_\infty S}{4m}\left[C_D - C_{L_\alpha} + \frac{md^2}{I}\left(C_{m_q} + C_{m_{\dot{\alpha}}}\right)\right]$$

REFERENCES

1. Love, Eugene S.; Henderson, Arthur, Jr.; and Bertram, Mitchel H.: Some Aspects of Air-Helium Simulation and Hypersonic Approximations. NASA TN D-49, 1959.

2. Henderson, Arthur, Jr.: Recent Investigations of the Aerodynamic Characteristics of General and Specific Lifting and Nonlifting Configurations at Mach 24 in Helium, Including Air-Helium Simulation Studies. The High Temperature Aspects of Hypersonic Flow, Wilbur C. Nelson, ed., AGARDograph 68, Pergamon Press, 1964, pp. 163-190.

3. Harris, Julius E.: Force-Coefficient and Moment-Coefficient Correlations and Air-Helium Simulation for Spherically Blunted Cones. NASA TN D-2184, 1964.

4. Dayman, Bain, Jr.: Simplified Free-Flight Testing in a Conventional Wind Tunnel. Tech. Rep. No. 32-346 (Contract No. NAS 7-100), Jet Propulsion Lab., California Inst. Technol., Oct. 1, 1962.

5. Jaffe, Peter: Obtaining Free-Flight Dynamic Damping of an Axially Symmetric Body (at All Angles of Attack) in a Conventional Wind Tunnel. Tech. Rep. No. 32-544 (Contract No. NAS 7-100), Jet Propulsion Lab., California Inst. Technol., Jan. 15, 1964.

6. Holway, H. P.; Herrera, J. G.; and Dayman, B., Jr.: A Pneumatic Model Launcher for Free-Flight Testing in a Conventional Wind Tunnel. Tech. Mem. No. 33-177, Jet Propulsion Lab., California Inst. Technol., July 30, 1964.

7. Prislin, Robert H.: Free-Flight and Free-Oscillation Techniques for Wind-Tunnel Dynamic-Stability Testing. Tech. Rep. No. 32-878 (Contract No. 7-100), Jet Propulsion Lab., California Inst. Technol., Mar. 1, 1966.

8. Goetz, Robert C.: Effects of Leading-Edge Bluntness on Flutter Characteristics of Some Square-Planform Double-Wedge Airfoils at a Mach Number of 15.4. NASA TN D-1487, 1962.

9. Campbell, James F.; and Howell, Dorothy T.: Supersonic Aerodynamics of Large-Angle Cones. NASA TN D-4719, 1968.

10. South, Jerry C., Jr.: Calculation of Axisymmetric Supersonic Flow Past Blunt Bodies With Sonic Corners, Including a Program Description and Listing. NASA TN D-4563, 1968.

11. Margolis, Kenneth: Theoretical Evaluation of the Pressures, Forces and Moments at Hypersonic Speeds Acting on Arbitrary Bodies of Revolution Undergoing Separate and Combined Angle-of-Attack and Pitching Motions. NASA TN D-652, 1961.

12. Uselton, B. L.: Damping-in-Pitch Derivatives for 60- and 70-deg Blunted Cones at Mach Numbers 3 Through 5. AEDC-TR-69-119, U.S. Air Force, June 1969.

TABLE I.- MODEL PROPERTIES AND TEST CONDITIONS

[d = 0.25 ft (0.0762 m); S = 0.049 ft^2 (0.00455 m^2); C_{L_α} = -1.29 (from ref. 9)]

Case	m		x_{cg}	I		$\frac{I}{md^2}$	$p_{t,\infty}$		q_∞		C_D
	slugs	kg		slug-ft^2	kg-m^2		psi	kN/m^2	psf	N/m^2	
1	4.23×10^{-3}	0.0617	0.45	5.91×10^{-6}	8.04×10^{-6}	0.0224	262	1806.5	130	6224.4	1.55
2	5.42	.0791	.45	7.42	10.09	.0219	294	2027.1	146	6990.4	1.54
3	5.39	.0787	.50	7.77	10.57	.0231	294	2027.1	146	6990.4	1.57
4	5.39	.0787	.48	7.22	9.82	.0214	322	2220.1	160	7660.8	1.54
5	5.39	.0787	.48	7.20	9.79	.0214	313	2158.1	155	7421.4	1.56
6	3.36	.0490	.36	5.43	7.38	.0259	330	2275.3	164	7852.3	1.41
7	3.32	.0485	.36	4.74	6.45	.0228	313	2158.1	155	7421.4	1.38
8	3.32	.0485	.40	5.52	7.51	.0266	290	1999.5	144	6894.7	1.54
9	5.46	.0797	.48	8.12	11.04	.0238	234	1613.4	116	5554.1	1.76
10	3.27	.0477	.55	5.00	6.80	.0245	235	1620.3	117	5602.0	1.40

TABLE II. - SUMMARY OF STABILITY DATA

Case	n	ω, rad/sec	$\frac{\theta_n}{\theta_o}$	$\ln \frac{\theta_n}{\theta_o}$	$\overline{\theta}$, deg	C_{m_α}		$C_{m_q} + C_{m_{\dot{\alpha}}}$	
						Exp.	Theor.	Exp.	Theor.
1	3	279	0.8000	-0.2231	13.5	-0.288	-0.318	-0.624	-0.242
2	2	227	.8602	-.1506	4.32	-.213	-.318	-.579	-.242
3	2	245	.8827	-.1248	16.8	-.260	-.313	-.478	-.233
4	2	269	.8625	-.1480	14.9	-.266	-.316	-.596	-.236
5	2	258	.8333	-.1823	15.4	-.252	-.316	-.712	-.236
6	2	316	.8798	-.1284	17.2	-.269	-.333	-.470	-.259
7	2	300	.7643	-.2690	6.14	-.224	-.333	-.796	-.259
8	2	295	.8873	-.1195	5.90	-.272	-.327	-.477	-.251
9	2	223	.9487	-.0526	5.70	-.284	-.316	-.318	-.236
10	2	319	.8848	-.1224	20.8	-.354	-.306	-.563	-.223

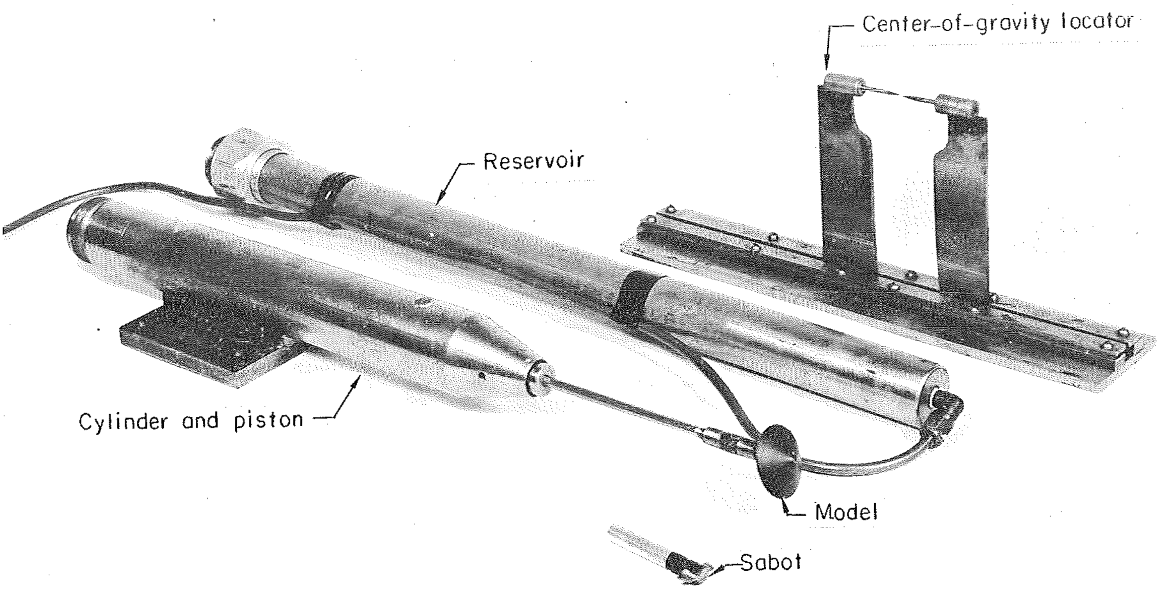

L-68-9087.1

Figure 1.- Model launcher and the device used to determine the center of gravity of the model.

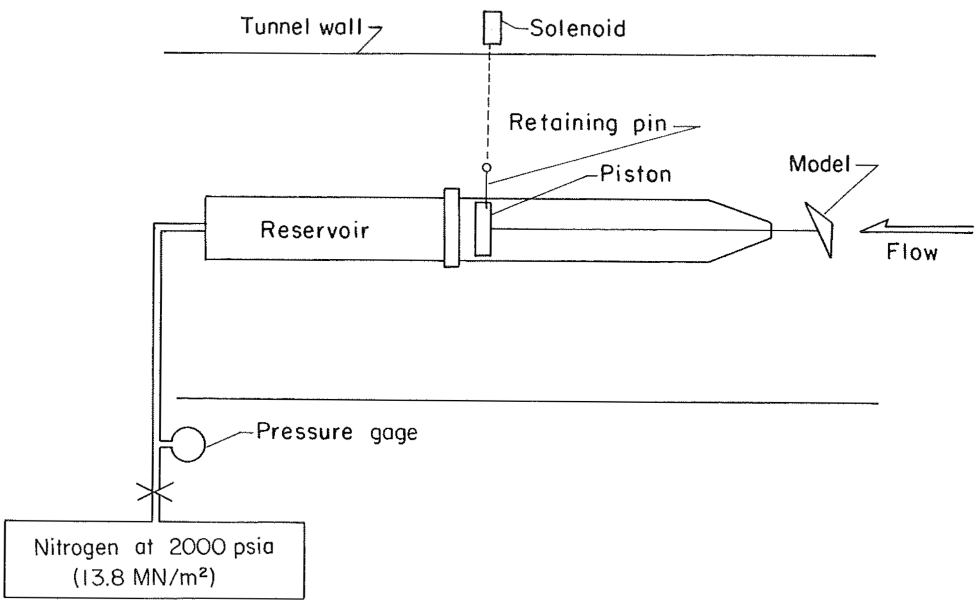

Figure 2.- Model launching system.

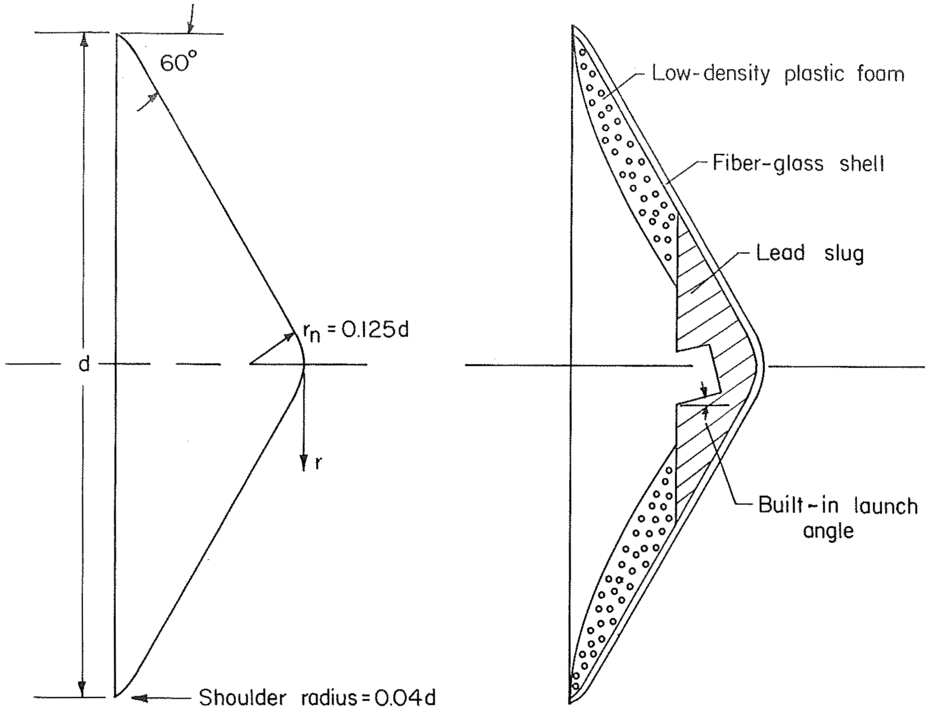

Figure 3.- Dimensions and construction of the models.

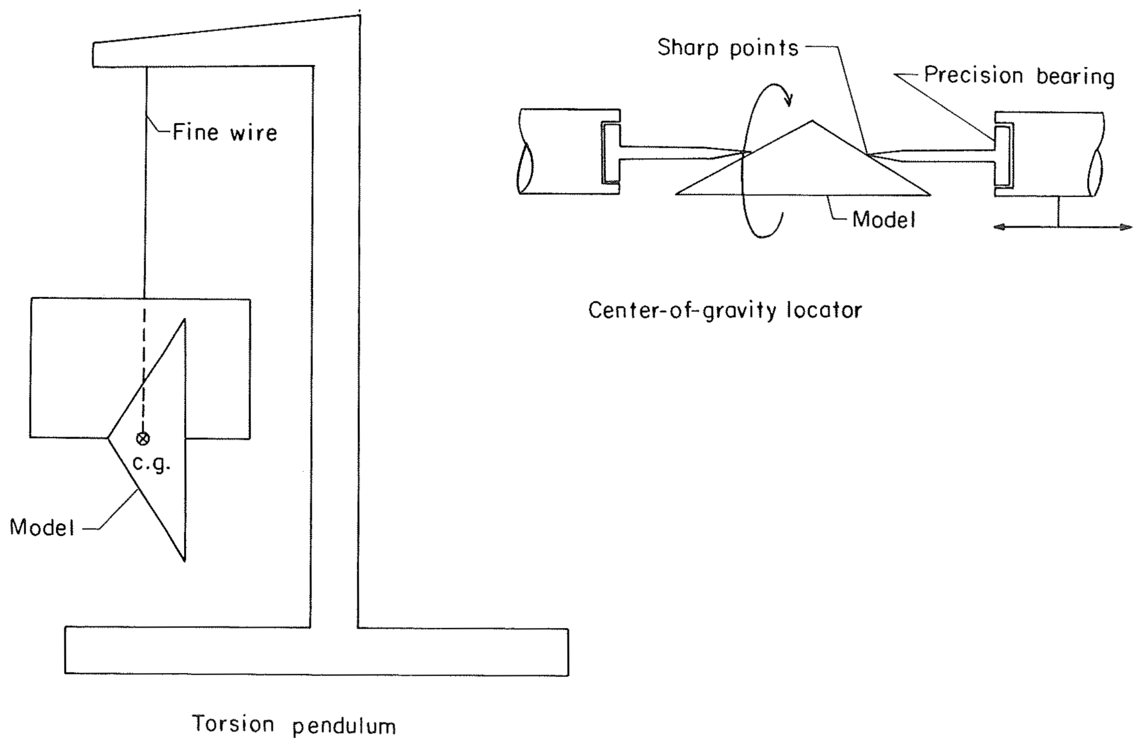

Figure 4.- Devices for measuring moment of inertia and locating center of gravity.

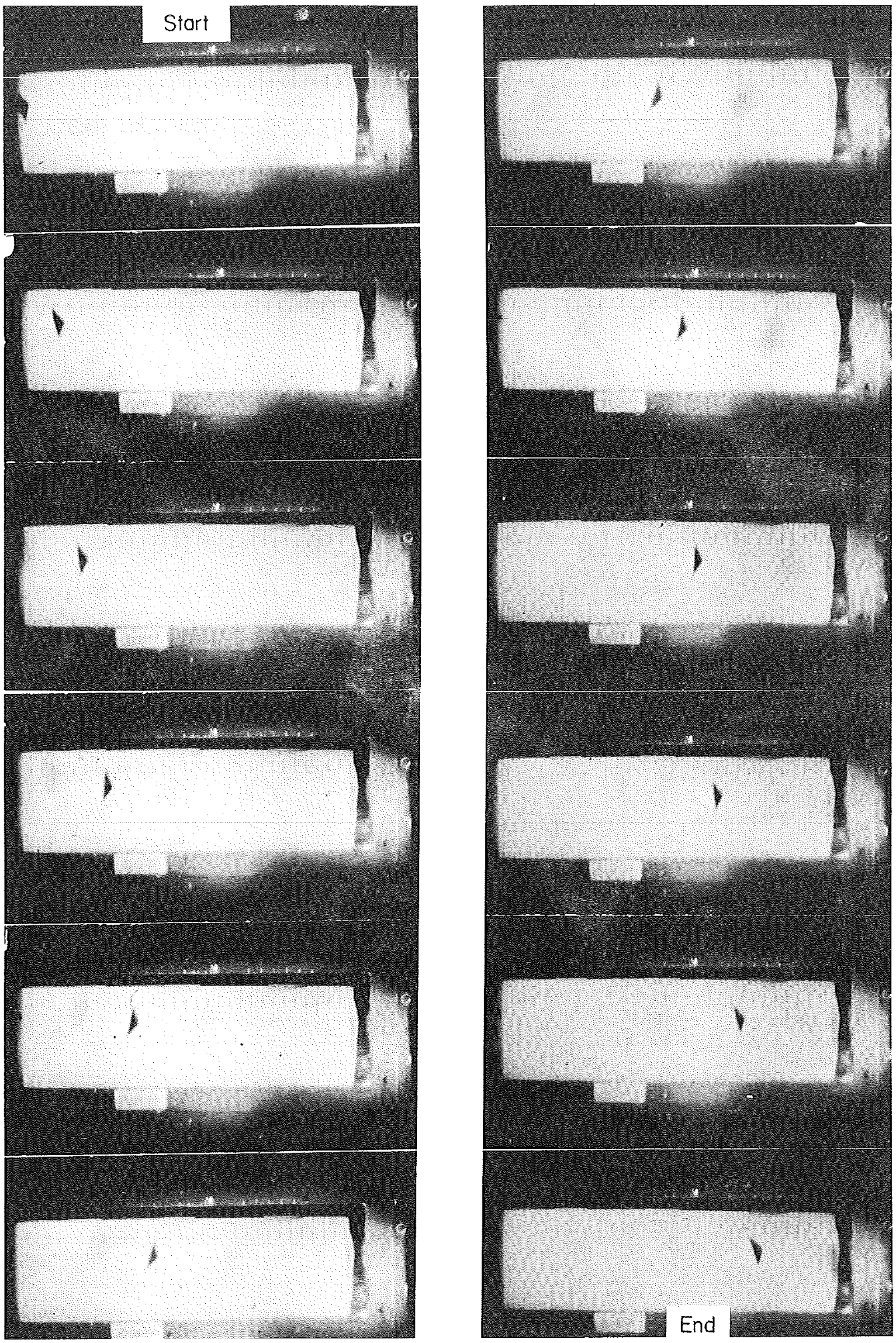

L-70-4743

Figure 5.- Photograph showing a typical flight upstream in the test section.

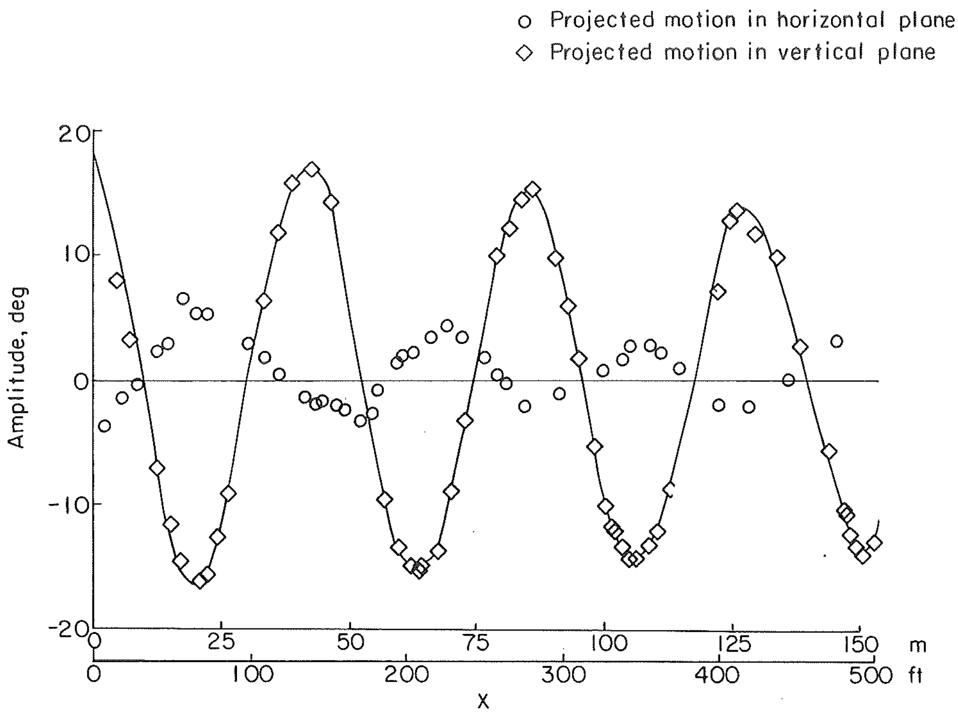

Figure 6.- Typical model motion in two orthogonal planes (case 5).

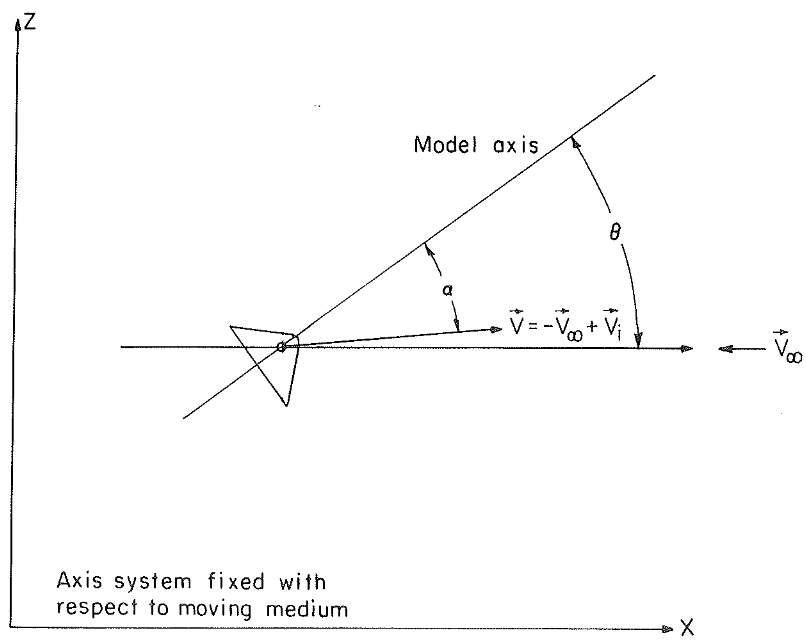

Figure 7.- Coordinate system.

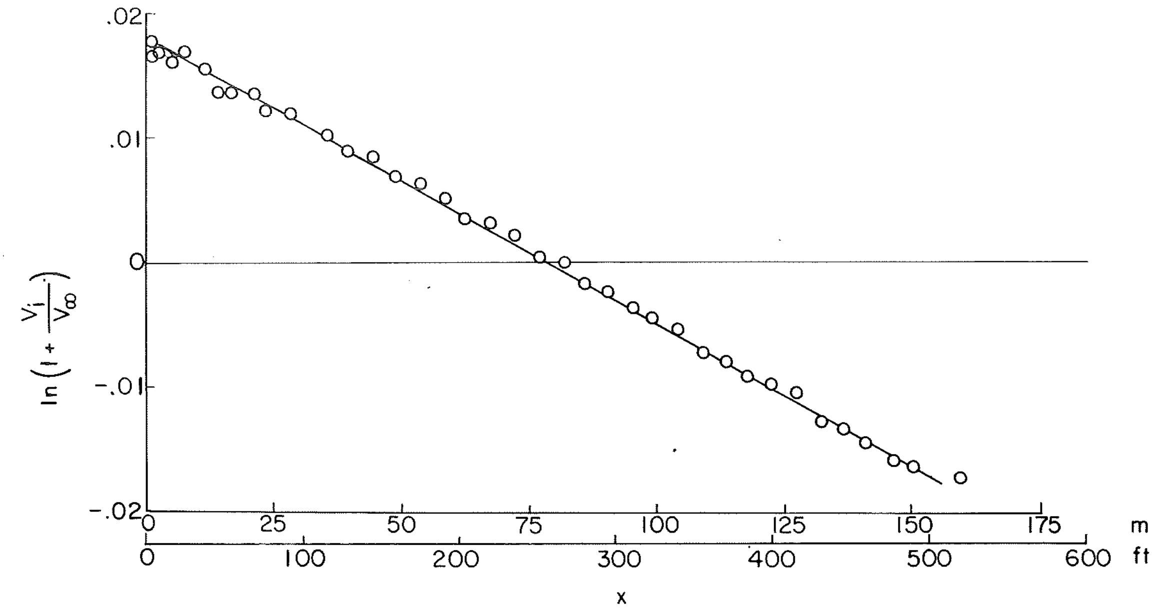

Figure 8.- Typical data used to determine drag (case 5).

$$C_D = -\frac{2m}{\rho_\infty S}\frac{d\left[\ln\left(1+\frac{V_i}{V_\infty}\right)\right]}{dx} = 1.56.$$

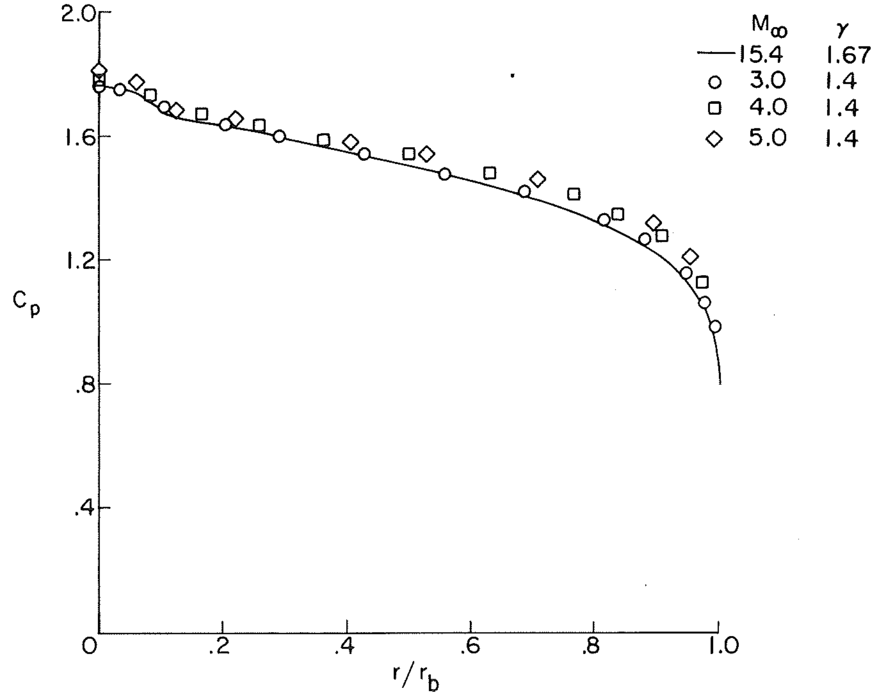

Figure 9.- Pressure distributions for 60° cone at zero angle of attack in air (γ = 1.4) and in helium (γ = 1.67), calculated by the method of integral relations (ref. 10).

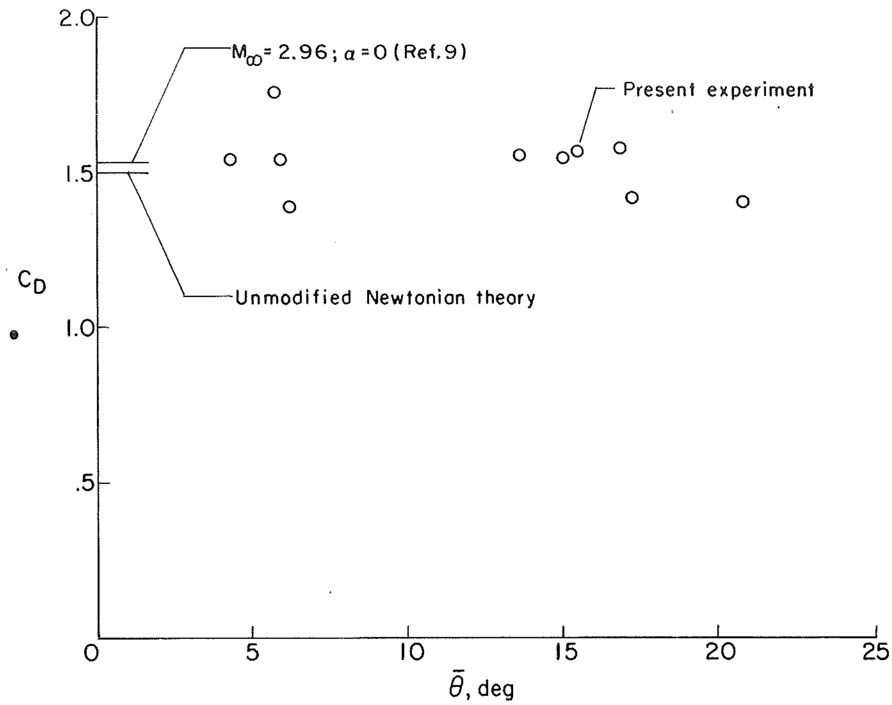

Figure 10.- Experimental and calculated values of the drag coefficient.

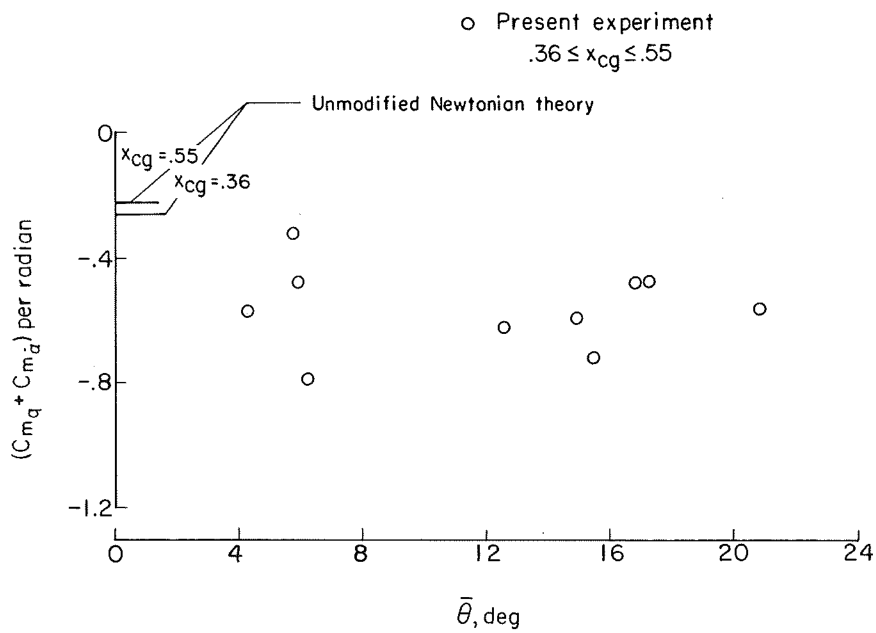

Figure 11.- Dynamic-stability coefficient as a function of root-mean-square amplitude. The theoretical values encompass the range of center-of-gravity locations of the experimental data.

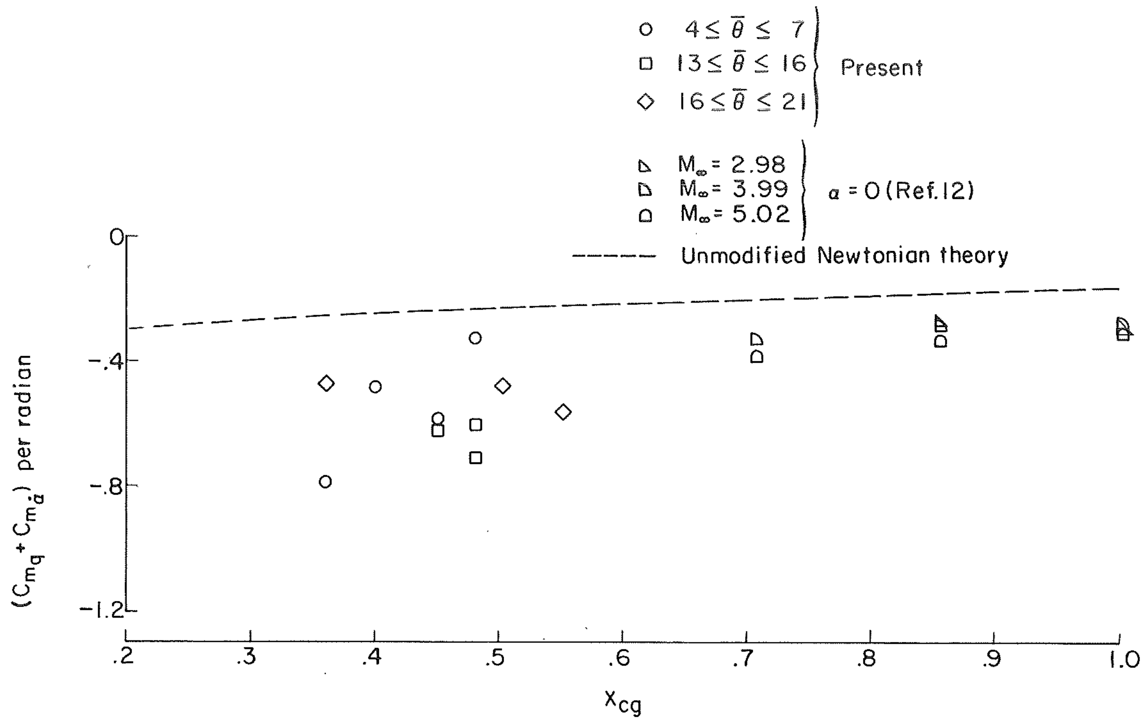

Figure 12.- Experimental and theoretical values of the dynamic-stability coefficient as a function of center-of-gravity location.

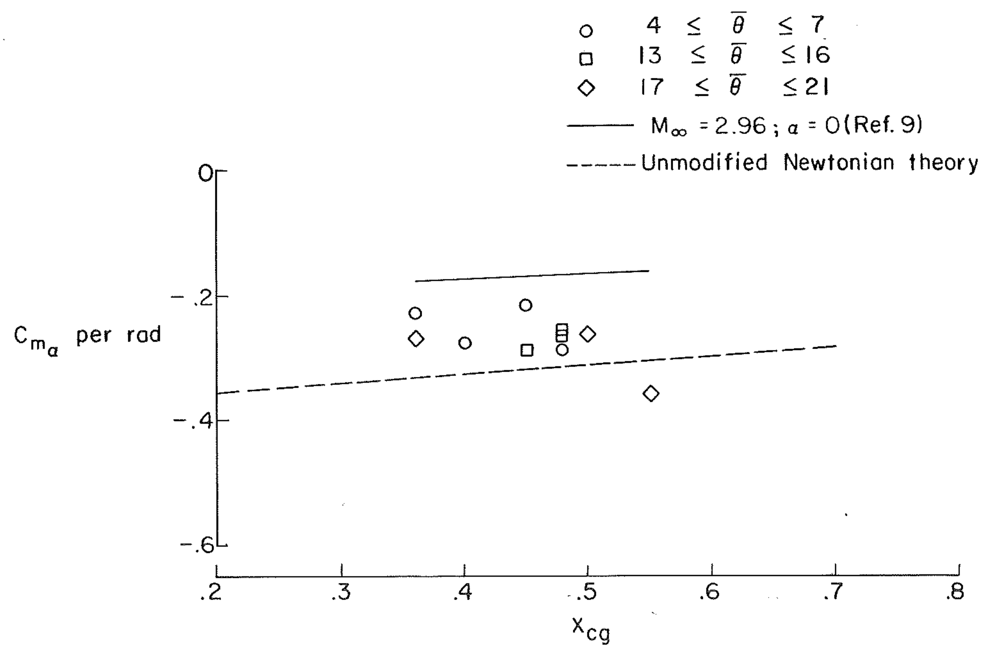

Figure 13.- Variation of experimental and theoretical values of static-stability coefficient with center-of-gravity location.

NASA-Langley, 1970 —— 1 L-6883

NATIONAL AERONAUTICS AND SPACE ADMINISTRATION
WASHINGTON, D. C. 20546

OFFICIAL BUSINESS

FIRST CLASS MAIL

POSTAGE AND FEES PAID
NATIONAL AERONAUTICS AND
SPACE ADMINISTRATION

POSTMASTER: If Undeliverable (Section 158 Postal Manual) Do Not Return

---

"The aeronautical and space activities of the United States shall be conducted so as to contribute . . . to the expansion of human knowledge of phenomena in the atmosphere and space. The Administration shall provide for the widest practicable and appropriate dissemination of information concerning its activities and the results thereof."

— NATIONAL AERONAUTICS AND SPACE ACT OF 1958

NASA SCIENTIFIC AND TECHNICAL PUBLICATIONS

TECHNICAL REPORTS: Scientific and technical information considered important, complete, and a lasting contribution to existing knowledge.

TECHNICAL NOTES: Information less broad in scope but nevertheless of importance as a contribution to existing knowledge.

TECHNICAL MEMORANDUMS: Information receiving limited distribution because of preliminary data, security classification, or other reasons.

CONTRACTOR REPORTS: Scientific and technical information generated under a NASA contract or grant and considered an important contribution to existing knowledge.

TECHNICAL TRANSLATIONS: Information published in a foreign language considered to merit NASA distribution in English.

SPECIAL PUBLICATIONS: Information derived from or of value to NASA activities. Publications include conference proceedings, monographs, data compilations, handbooks, sourcebooks, and special bibliographies.

TECHNOLOGY UTILIZATION PUBLICATIONS: Information on technology used by NASA that may be of particular interest in commercial and other non-aerospace applications. Publications include Tech Briefs, Technology Utilization Reports and Notes, and Technology Surveys.

Details on the availability of these publications may be obtained from:

SCIENTIFIC AND TECHNICAL INFORMATION DIVISION

NATIONAL AERONAUTICS AND SPACE ADMINISTRATION

Washington, D.C. 20546